Auger Electron Spectroscopy: A Rational Method for Determining Thickness of Graphene Films

Mingsheng Xu,[†,‡,*] Daisuke Fujita,[§] Jianhua Gao,[§] and Nobutaka Hanagata[⊥]

[†]International Center for Young Scientists, National Institute for Materials Science, 1-2-1 Sengen, Tsukuba, Ibaraki 305-0047, Japan, [‡]Department of Polymer Science and Engineering, State Key Laboratory of Silicon Materials, and Key Laboratory of Macromolecule Synthesis and Functionalization, Zhejiang University, Hangzhou 310027, People's Republic of China, [§]Advanced Nano Characterization Center and International Center for Materials Nanoarchitectonics, National Institute for Materials Science, 1-2-1 Sengen, Tsukuba, Ibaraki 305-0047, Japan, and [⊥]Nanotechnology Innovation Center, National Institute for Materials Science, 1-2-1 Sengen, Tsukuba, Ibaraki 305-0047, Japan

ABSTRACT We report the determination of the thickness of graphene layers by Auger electron spectroscopy (AES). We measure AES spectra of graphenes with different numbers of layers. The AES spectroscopy shows distinct spectrum shape, intensity, and energy characteristics with an increasing number of graphene layers. We also calculate electron inelastic mean free paths for graphene layers directly from these measurements. The method allows unambiguous and high-throughput determination of thickness up to six graphene layers and detection of defect and dopant in graphene films on almost any substrate. The availability of this reliable method will permit direct probing of graphene growth mechanisms and exploration of novel properties of graphenes with different thicknesses on diverse substrates.

KEYWORDS: graphene · thickness · layers · Auger electron spectroscopy · Raman spectroscopy

Graphene systems, consisting of one or a few crystalline monolayers of carbon atoms tightly packed into a two-dimensional (2D) honeycomb lattice, stand out because of their extraordinary optical and electronic properties and their potential applications in nano-optoelectronic devices.[1,2] The optical and electronic properties of graphenes rely heavily on the number of graphene layers, dopant, defect, and coupling with the underlying substrate. It has been pointed out that monolayer (ML), bilayer (BL), and trilayer (TL) graphenes show different electronic properties from each other,[2−11] and the electronic structure rapidly evolves with the number of layers, approaching the three-dimensional (3D) limit of graphite at ~10 layers.[2,3] Thus, identification of the number of graphene layers (*i.e.*, determination of their thickness) is essential for informed research.

The development of graphene-based technology relies on its detection techniques. As for nanoscale thickness metrology of graphenes, various methods, including atomic force microscopy (AFM), optical microscopy,[12−14] contrast spectroscopy,[15] confocal Rayleigh scattering microscopy,[16] and Raman spectroscopy,[17−23] are used to count graphene layers. Low-energy electron diffraction and angle-resolved ultraviolet photoemission spectroscopy have been demonstrated to be capable of distinguishing graphene films up to three layers on SiC.[24] Among these, Raman spectroscopy[17−19,25] has grown into a rapid and powerful tool to characterize graphene layers in ambient air for the past several years. Raman scattering can not only identify the number of graphene layers but also detect charge impurities,[26,27] structural defects,[17] edge states,[28,29] and strain effects,[30] determine crystalline orientations[31] and stacking order,[32] and investigate electron−photon coupling of biased graphene.[33,34] However, most Raman spectroscopic studies of graphene have been carried out for graphene on standard SiO_2/Si substrate with 300 nm thickness of the oxide layer.[17−23,25−34] The Raman spectra of graphenes on GaAs,[19] SiC,[24] glass,[25] and Cu[35] are complicated by the effect of the substrates. Furthermore, monolayer graphene on some substrates, such as Ru[36] and Ni,[37] shows no detectable Raman characteristics. This is mainly due to the relatively strong electronic coupling between the graphene and the substrates, and thus the π bonds soften in graphene.[38] Growth of graphene films on SiC,[24] Ni,[39−41] and Cu[42,43] is promising for producing large-scale graphenes for practical applications. It would be desirable to directly characterize the graphene films on these substrates, rather than transferring the formed

*Address correspondence to xu.mingsheng@nims.go.jp.

Received for review February 9, 2010 and accepted April 02, 2010.

Published online April 7, 2010.
10.1021/nn100276w

graphene films onto other substrates such as SiO_2/Si to understand the growth mechanisms, structural defects, and quality because the transfer procedures may damage delicate graphenes,[35] and such post-investigation may not reveal the real nature of synthesized graphenes for understanding growth mechanisms and optimizing growth procedures. Therefore, a technique, suitable for many important substrates, for determining thickness of graphene films is urgently needed because of the rapid development of this field and because the unique properties of graphene systems are strongly dependent on the thickness and interaction with the underlying substrate.

Auger electron spectroscopy (AES) is a standard and powerful surface analytical technique based on the analysis of energetic electron emitted from an excited atom after a series of internal relaxation events. It enables one to explore the first few atomic layers and map elemental distributions with high spatial resolution and precise chemical sensitivity.[44] Previously, AES was employed to study the monolayer phase of graphite on various substrates such as Ni[45−47] and few-layer graphene on SiC.[23,48] However, the electron inelastic mean free paths (IMFPs) used in those studies were not from graphenes, and there was no systematic investigation. Here we report on a direct, efficient, and accurate method for determining the thickness of graphene layers on almost any substrate based on AES technique. We also calculate the IMFPs of Auger electrons for graphenes as a function of electron energy. Compared with other methods with limitation to some substrates, this AES method provides a direct, efficient, and more universal means of quickly yielding accurate knowledge of graphene system thickness on almost any substrate. It can detect impurity and structural defect and possibly monitor *in situ* the formation of graphenes, which dictates the properties and growth mechanisms of the materials and consequently speeds up research and application of graphene-based materials that are required.

RESULTS AND DISCUSSION

Figure 1a shows the optical image of a graphene sample on a Si ⟨100⟩ substrate covered with a 300 nm SiO_2 layer prepared by the micromechanical cleavage method. The graphene sheet shows different contrast regions in color, which indicate different thicknesses (Figure 1a). Raman spectra were taken in different areas of the sample, and the results are plotted in Figure 1c. The two most noteworthy features are the G peak at ~1584 cm^{-1} and the 2D band at ~2662−2686 cm^{-1}. Especially striking in the monolayer graphene is the single, sharp, and symmetric 2D peak that differs from the spectra obtained from bilayer and few-layer graphenes. For bilayer and few-layer graphenes, the 2D band is much broader and exhibits no obvious differences, mainly due to the change of electronic structures, which affects the process of the double resonance effect.[17] Clear differences between the bilayer and few-layer graphenes are the upshift of the 2D peak position and the intensity of G band increasing with the number of layers. As elucidated by Ferrari *et al.*,[17] for more than five layers, the Raman spectrum becomes hardly distinguishable from that of bulk graphite. Thus, Raman spectroscopy can clearly distinguish a single layer from a bilayer from few (<5) layers.

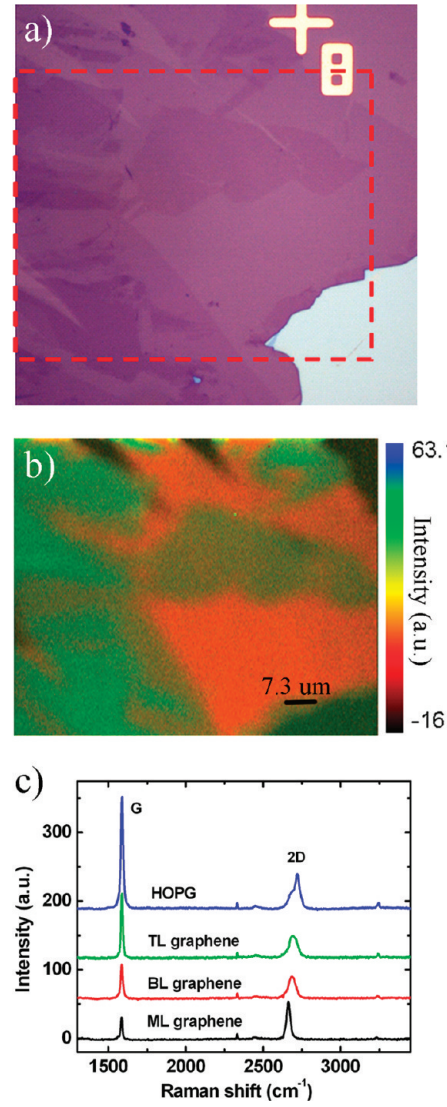

Figure 1. Characterization of graphene layers on SiO_2/Si substrate. (a) Optical microscope image of an exfoliated graphene flake containing monolayer, bilayer, and trilayer graphenes. The numbers indicate the number of graphene layers. (b) Raman image immerged with the intensity of G and 2D bands acquired in the rectangular region in (a). (c) Raman spectra as a function of the number of graphene layers. The intensity of the G peak increases with more layers of graphene, whereas the 2D band shows an upshift in position.

Figure 2 shows the Si LVV, C KLL, and O KLL AES spectra of the same graphene sample on a SiO_2 surface (see Figure 3). These primary AES spectra show distinct characteristics in peak shape, peak intensity, and kinetic energy with the change of the number of graphene layers. It is clear that the intensity of the

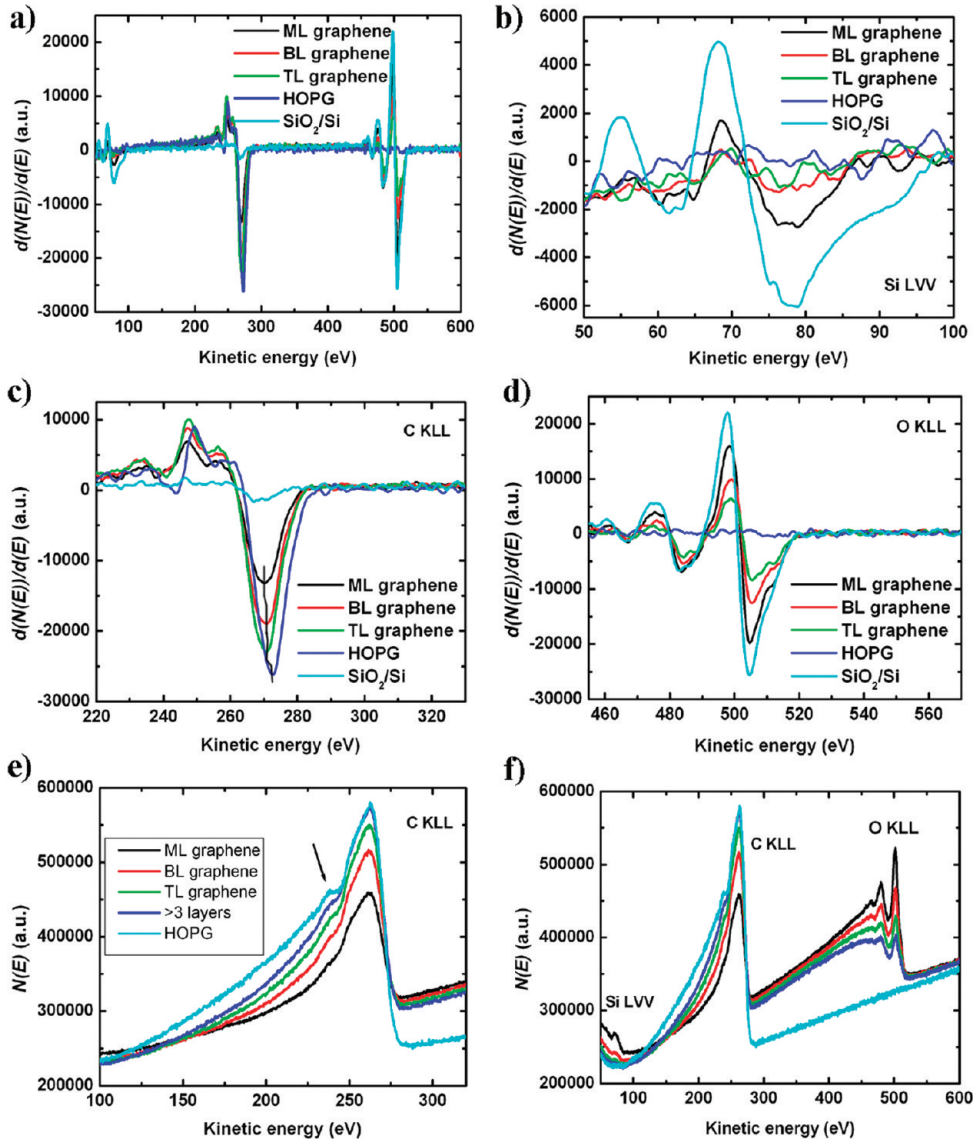

Figure 2. AES spectra of graphene layers on SiO_2/Si substrate acquired from the same sample as in Figure 1. Spectra in a−d are the first differential AES spectra ($d(N(E))/d(E)$) calculated from the direct AES spectra ($N(E)$) in e and f. (a) Survey spectra at the kinetic energy range from 50 to 600 eV with an energy step of 0.2 eV. (b) Si LVV electron spectra. (c) C KLL electron spectra. (d) O KLL electron spectra. The Si LVV and O KLL Auger electron intensity was attenuated with an increase in the layers of graphenes, whereas that in the C KLL electron increased. (e) Direct C KLL electron spectra, highlighting evolution of the peak at ~240 eV with a decrease in the number of graphene layers. (f) Direct survey spectra at the kinetic energy range from 50 to 600 eV. The inelastic background signal around the O KLL peak increased with an increase in the layers of graphenes. The different colored spectra are corresponding to those in e.

Si LVV (Figure 2b) and O KLL (Figure 2d) Auger electron transitions observed from the SiO_2 substrate gradually became attenuated, whereas that of C KLL (Figure 2c) transition from the graphene layers increased with a higher number of graphene layers. Although there was no shift of the O KLL peak (Figure 2d), the C KLL peak (Figure 2c, negative peak in the first differential spectrum: $d(N(E))/d(E)$) was found to have shifted from 273.0 eV (HOPG, *i.e.*, highly oriented pyrolytic graphite), 270.6 eV (trilayer), 270.4 eV (bilayer), to 270.2 eV (monolayer) to a lower kinetic energy position with a decreasing number of graphene layers. Moreover, the C KLL AES spectra (Figure 2c,e) show evolution of the peak structure at ~240 eV ($N(E)$, direct spectra) as pointed with arrow in Figure 2e. This peak in the C KLL AES spectrum of HOPG became weak and disappeared in the graphenes with a decrease in the number of layers (also see Supporting Information). In addition, the inelastic background signal around the O KLL peak increased with an increase in the number of graphene layers (Figure 2f).

The peak structure at ~240 eV of the C KLL spectrum of HOPG and graphite is well-known,[49] but such an evolution with the number of graphene layers has not been reported before, and the origin of the peak is unclear. In graphite, the sp^2 ($s\text{-}p_x\text{-}p_y$) hybridization of atomic orbitals (denoted σ) forms a covalently bound lattice of a graphene sheet, which is weakly bound by

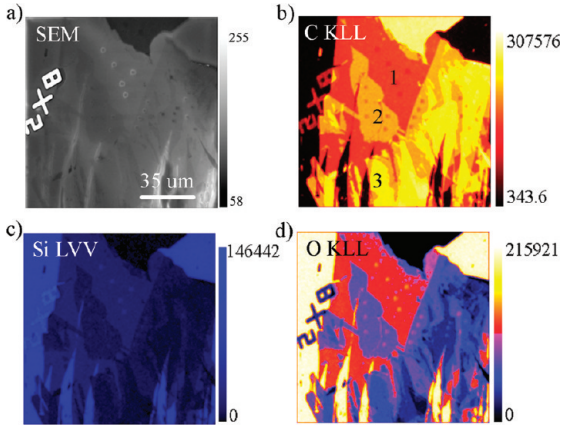

Figure 3. Auger element maps of graphene layers on SiO_2/Si substrate showing the same sample region as in Figure 1. (a) Scanning electron image showing a strong contrast of secondary electron emissions from the different layers of graphenes. (b) C KLL electron map showing striking intensity contrast among the monolayer, bilayer, trilayer, and thicker graphenes. (c) Si LVV electron map showing the intensity was gradually attenuated with an increase in graphene layers. (d) O KLL electron map showing the intensity increases with a decrease in graphene layers. The dot-shaped spots were left after we performed an electron beam damage study.

the residual forces from the nonhybridized p_z orbitals (denoted π) perpendicular to the planes. There are six σ and two π energy bands in the valence band.[50] They are doubly degenerate in the monolayer graphene sheet. The two π states can be further denoted as π_s and π_{int}. The π_s is a state similar to that in a single graphene sheet, and π_{int} is a state closest to the Fermi level, that is, the upper π-band, which overlaps along the Brillouin zone edges HKH and H'K'H'.[51] Given that, in the first approximation, the C KLL line shape is a self-fold of valence band density of states, and its intensity can be expressed by[50,51]

$$I \sim (\sigma + \pi_s + \pi_{int})^*(\sigma + \pi_s + \pi_{int})$$
$$= \sigma^*\sigma + 2\sigma^*\pi_s + 2\sigma^*\pi_{int} + \pi_s^*\pi_s + 2\pi_s^*\pi_{int} + \pi_{int}^*\pi_{int} \quad (1)$$

where * denotes a self-fold procedure. It is well-known that π_{int} is induced by interlayer interaction.[50,51] Thus, on the basis of our observation of the evolution of the peak at ~240 eV, we can attribute the terms involved with π_{int} to the origin of the peak and other terms to the main peak at ~273 eV. Therefore, these features reflect a different chemical environment of the Auger electron and electronic interaction among the layers and with the substrate.

Figure 3 displays the Auger electron element maps. These Auger maps show a pronounced contrast between graphenes with different numbers of layers. The high resolution of AES may directly resolve defects seen as dot-shaped spots, which were left after we assessed a possible electron beam irradiation effect on graphenes.[52] Note that the spectra in Figure 2 were obtained with optimized experimental conditions and prior to the irradiation damage assessment and were not exposed to focus electron beam except for acquiring a scanning electron image. It was found that damage depended on electron beam energy and exposure dose. This suggests that, similar to Raman measurement,[52] beam energy and exposure dose of AES measurement should be optimized for reproducible characterization to avoid local energy stimulated damage to graphenes. As a result, the AES technique provides a wealth of information about physical, chemical, and electronics properties of the graphene systems.

We then calculated the electron IMFPs for graphene systems directly from the Auger measurement based on common attenuation models. The IMFP (λ) is a key material parameter in AES and X-ray photoelectron spectroscopy, as well as in other techniques involving electron scattering or emission at a solid surface.[53] In estimating λ with the C KLL Auger electron transition, we assumed that there was no inelastic attenuation in the outermost graphene layer and neglected the possible diffraction effect from the graphene crystalline surfaces. Thus, the intensity of the C KLL Auger electron from the *n*th-layer graphene can be expressed by[44]

$$I_n = I_0 \Sigma \exp[-(n-1)d_0/\lambda \sin(\theta)] \quad (2)$$

where I_n is the intensity of the C KLL Auger electron from the *n*th-layer graphene; I_0 is the intensity of the Auger electron from the outermost layer of graphene; d_0 is the thickness of graphene (0.335 nm); θ is the electron takeoff angle (42°) of the present Auger instrument; and λ is the inelastic mean free path of the Auger electron for graphene systems. In the case of estimating λ with the Si LVV and O KLL transitions, we assumed that the inelastic attenuation was caused by graphene layers and neglected the effect of SiO_2 layer and diffraction effect. Thus, the intensity of the Si LVV and O KLL Auger electron after attenuation by the graphene layers can be given by[44]

$$I_{sub} = I_{sub,pure} \exp[-(nd_0)/\lambda \sin(\theta)] \quad (3)$$

where I_{sub} is the intensity of the Si LVV or O KLL Auger electron from the SiO_2 substrate covered with graphene layers; $I_{sub,pure}$ is the intensity of the Si LVV or O KLL Auger electron from the pure SiO_2 without graphene overlayers; and *n* is the number of graphene layers.

The IMFPs for graphene systems derived from the Si LVV, C KLL, and O KLL transitions in monolayer, bilayer, and trilayer graphenes are plotted in Figure 4a, together with the values calculated for graphite with the Tanuma, Powell, and Penn (TPP)-2 predictive formula[54] at the energy of Si LVV peak and C KLL peak (see Supporting Information). The two values for graphite are close to our estimation for graphenes. Furthermore, our values are found to be between the IMFPs calculated for glassy carbon from optical data and the estimation with the TPP-2 predictive formula[54] as a function of

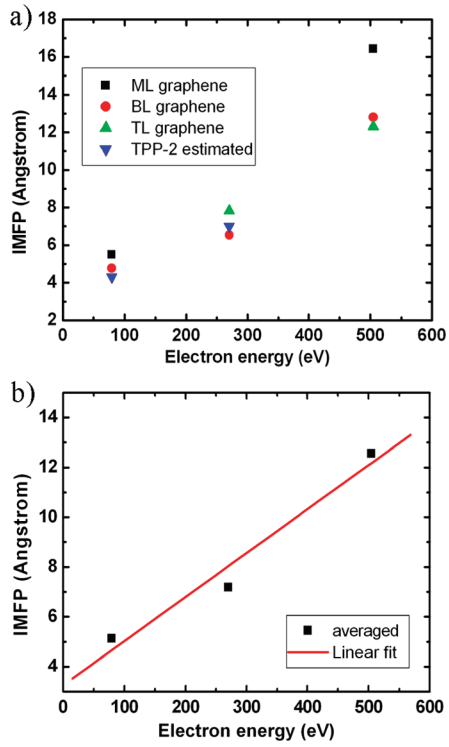

Figure 4. Electron inelastic mean free paths for graphenes as a function of electron energy derived from AES characterization. (a) Values were calculated by using the peak-to-peak intensity of the $d(N(E))/d(E)$ spectra in Figure 2. (b) IMFPs averaged from the monolayer, bilayer, and trilayer graphenes and linear fit of the averaged values.

electron energy. The IMFPs calculated using optical data have an uncertainty of ~10% associated with the typical uncertainty of the optical data. The TPP-2 formula for predicting absolute IMFPs also has limitations, such as uncertainties associated with the theory and the choice of parameters.[54] Additionally, the IMFPs obtained by both estimations represent inelastic scattering in bulk materials rather than surface layers. In our calculation, we did not consider the diffraction of the crystalline graphene layers and neglected the attenuation in the outermost graphene layer or the SiO_2 of the Auger electrons. Our IMFP values derived from the monolayer, bilayer, and trilayer graphenes at the fixed energies show good consistence, except that calculated from the O KLL Auger electron transition in the monolayer graphene. Although the reason is not clear at the moment, the deviation may be due to interface diffraction and the two-dimensional nature of graphene. Note that the currently available IMFPs in literature are all for three-dimensional bulk materials.

Once the IMFPs for graphenes are established, we can estimate the maximum number (or thickness) of graphene layers that could be identified by the AES technique using either eq 2 or eq 3. For a simplification, we used the fit IMFPs from the IMFP values (Figure 4b) averaged from the monolayer, bilayer, and trilayer graphenes excluding the IMFP value derived from O KLL Auger electron for monolayer graphene. We linearly fit the averaged IMFPs because almost linear behavior of IMFP for glassy carbon as well as many other solids is obtained as a function of electron energy (>50 eV) according to TPP-2.[54] By measuring the intensity of the C KLL Auger electron transition from a pure HOPG under the same conditions as the measurement of graphenes, and applying it and the linearly fit IMFP value (8.0 Å) at the C KLL electron energy to eq 2, we could discriminate a total of six layers of graphene by assuming the identical distance (3.35 Å) of the graphene interlayers. Various thickness of monolayer graphene on SiO_2/Si substrates was reported by AFM measurement in ambient air, and difference explanations such as adsorbed molecules,[18] instrumental factors,[52,55] and ripples in graphene were given. The AES measurement was carried out in ultrahigh vacuum (~1.0×10^{-10} Torr). On the other hand, when we applied the O KLL noise level from pure HOPG, the intensity of the O KLL Auger electron from pure SiO_2, and the IMFP value of ~12.1 Å at the electron energy of O KLL to eq 3, we could theoretically determine the maximum thickness equivalent to ~7.5 layers of graphene. Compared to six layers, a larger number estimated by using O KLL signal may be due to the fact that we used the noise level O KLL Auger electron of HOPG as the minimum signal detected, and Auger electron with low kinetic energy is more sensitive to surface and structure changes than with higher kinetic energy. The signal-to-noise ratio can be improved by increasing spectrum acquiring cycle. In this work, we used four cycles. Thus, we believe that the AES method is capable of determining the thickness up to six layers of monolayer graphene.

To confirm the reliability of the AES method, we demonstrate its reproducibility and accuracy by measuring monolayer graphene synthesized on Ni substrate. We can produce large-scale and uniform graphene on Ni substrate. The graphene on Ni substrate does not shown any Raman characteristics between 1000 and 3500 cm^{-1} by using 532 and 514 nm excitation lasers but could discriminate it as monolayer graphene after it is transferred onto a SiO_2/Si substrate. Different measurement runs (see Supporting Information) of a same sample under the same measurement conditions generated identical spectrum characteristics. Furthermore, the Auger spectrum of the monolayer graphene shows very similar C KLL features, weakened peak at ~240 eV compared to that of HOPG, to that on the SiO_2 (Figure 2e as well as Supporting Information). This suggests that it may be possible to distinguish the number of graphene layers only by the evolution of the peak structure at ~240 eV of C KLL Auger spectrum. Now, we determine the thickness of a monolayer graphene synthesized on Ni substrate to evaluate accuracy of the AES method. We used eq 3, the IMFP value of ~4.45 Å (Figure 4b) at the energy of Ni MVV Auger electron and the Ni MVV peak-to-peak intensity (Figure

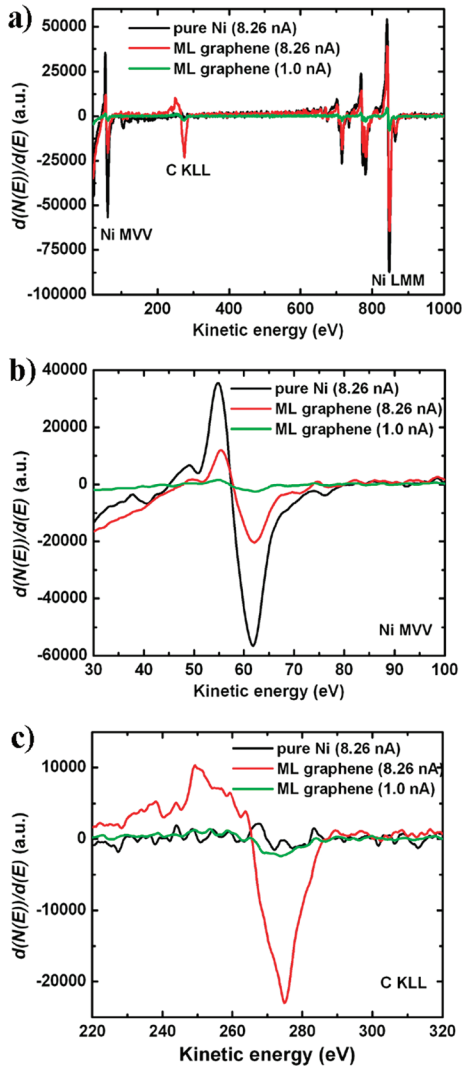

Figure 5. Accurate AES method for determining thickness of graphene films. (a) Survey AES spectra of a monolayer graphene on Ni substrate. The red and green electron spectra were obtained from a same uniform monolayer graphene on Ni substrate with different electron beam currents of ~8.26 nA (red curve) and 1 nA (green curve) and other measurement conditions kept the same, showing the dependence of Auger electron intensity on electron beam current. The black curve was obtained from pure Ni sample with the same measurement condition as that for the red curve. (b) Ni MVV AES spectra. (c) C KLL AES spectra.

5). Thus, we obtained 3.0 Å of the thickness of graphene on the Ni substrate. This value is smaller than the interlayer spacing (3.35 Å) of C−C distance; however, it is reasonable by considering the interfacial orbital hybridization between graphene and Ni[38,56,57] and the possibility to transfer graphene grown on Ni substrate to other substrates only by etching the Ni layer.[35] In addition, as seen in Figure 5 (also see Supporting Information), electron beam current density affects peak-to-peak intensity, underscoring the importance of optimized characterization.

Besides the thickness estimation models elucidated in this work, de Heer *et al.*[58] estimated the thickness of graphene layers synthesized on SiC based on the Si:C Auger intensity; we have also estimated graphene thickness synthesized on $Pt_{83}Rh_{17}$ surface based on the Pt:C Auger intensity,[59] though the IMFP value used for the thickness calculation was not for graphene. We show, in Supporting Information, AES spectra of graphene films with different coverages synthesized on Pt(111) and SiC(0001) substrates, as well as a graphene film transferred onto SiO_2/Si from a Ni substrate. All of these results demonstrate AES as a more universal technique for determining thickness of graphene films than Raman spectroscopy in the respect to the suitability for almost any substrate as well as high resolution to examining uniformity. Furthermore, Auger spectroscopy can detect impurity or dopant in graphenes. This is demonstrated by quantitatively detecting the Fe impurity trapped within the interfacial space between the transferred graphene and SiO_2/Si substrate from a Ni substrate (see Supporting Information). It is well-known that monolayer, bilayer, and trilayer graphenes each show unique electronic properties. We believe that few-layer graphenes (4−6 layers) also have unique properties because they still exhibit the 2D material system. Furthermore, mass production of graphenes with fine thickness control is still one major challenge of graphene-based technologies. Thus, AES could help to clarify the particular interesting properties of graphene systems with regard to the specific number of layers and to understand the growth mechanism and in turn guide formation of high-quality graphenes. For determination of the thickness of graphenes by the AES method, one only needs to calibrate a pure HOPG sample and/or a pure substrate used for growth of graphenes under the same conditions as the measurement of graphenes and apply the intensities to the eq 2 or 3.

CONCLUSION

In summary, we have demonstrated quantitative determination of the thickness of graphene films by using AES. We have also derived the IMFP values for graphenes as a function of electron energy directly from AES measurement. Auger spectra of graphenes show distinct fingerprints with a decrease in the number of graphene layers. AES is a direct and reliable technique that can quickly detect monolayer graphene and even the existence of strong electronic coupling with underlying substrate, determine thickness of graphene films up to six layers, directly see structural defects, and quantitatively detect chemical impurity/dopant on almost any substrate. Thus, together with Raman double-resonance scattering technique, Auger electron spectroscopy can help reveal interesting properties of 2D graphene systems and accelerates the application of graphenes for high-density graphene arrays with unique properties.

EXPERIMENTAL METHODS

Graphene Fabrication: Graphene flakes on ~300 nm dry thermal SiO_2 were purchased from Graphene Industries Ltd. and produced by the mechanical exfoliation method. The number of graphene layers was first estimated from the color contrast of the optical images by Graphene Industries Ltd., and we further confirmed their number by Raman spectroscopy. Graphenes on Ni, SiC, and Pt substrates were prepared by modified chemical vapor deposition, thermal annealing, and segregation methods, respectively. Future publications by us will detail the production methods and thickness determination.

Raman Spectrum Measurement: Raman spectra were recorded with a RAMAN-11 system (Nanophoton Corp., Japan), which illuminates a line-shaped area on the sample with a line-shaped laser beam. Raman scattering light from the line-shaped area on the sample was simultaneously detected by a parallel detection system. The scattering signal was dispersed with a Czerny−Turner-type spectrometer (f = 500 mm, the focal length of the spectrometer) and detected with an electrically cooled charge-coupled device (CCD) detector (400 × 1340 pixels). The excitation source was a 532 nm laser with a power setting <1.8 mW to avoid laser-induced damage. The lateral resolution was ~350 nm focused by a 100× optical lens (numerical aperture of 0.9), and the spectral resolution was ~1.6 cm^{-1}.

AES Characterization: AES measurements were performed at room temperature with a scanning Auger electron spectroscope (ULVAC-PHI model SAM650)[60] with a cylindrical mirror analyzer. The takeoff angle of the instrument was 42°. AES spectra were acquired with a primary electron beam of 10 kV. Except for the difference of electron beam current, other measurement conditions remained unchanged for all of the measurements. The incident electron beam current for the AES spectra displayed in Figure 2 was about 8.23 nA, as calibrated with a Faraday cup before and after each measurement. The direct Auger spectra were averaged from three different sample regions (~5.1 μm^2) on graphenes with different layers. The electron beam currents for AES measurements of the graphenes on the Ni, Pt, and SiC substrates, as well as pure HOPG and Ni, were specified in the captions of the figures. The measurement conditions of AES spectra presented in a same figure were kept the same except as specified elsewhere.

We used differential energy spectrum to subtract background from the direct Auger spectrum for calculating the peak-to-peak intensity. The first differential $d(N(E))/d(E)$ Auger spectra were obtained by numerical derivation of the direct $N(E)$ integrated Auger data displaying an absolute scale with counts/second unit by a universal Savitzky−Golay differential filter using five points and used to calculate the peak-to-peak intensity of Auger electrons and derive the number of graphene layers. The differential spectrum is simply the differential of the direct spectrum with respect to energy. The second differential $d^2(N(E))/d(E)^2$ spectrum is similarly done based on the first differential spectrum. In the differential energy spectrum, it has been customary to measure the peak-to-peak value of the signal. The peak-to-peak intensity, thus, is proportional to the absolute scale in the direct Auger spectrum. It is perfectly valid, and these values can be used for the calculation.[44] All of the AES spectra presented in this article were obtained with optimized experimental conditions to avoid effect induced by electron beam irradiation.

Key points for determining thickness of graphene films by AES metrology protocols are as follows: (1) preventing samples from contamination since it is almost impossible for AES to discriminate origins of carbons without careful analysis of chemical shift; note that graphene is impermeable to gases;[61] (2) choosing an appropriate electron beam current and a primary beam voltage; (3) measuring AES spectra with an appropriate measurement cycle at the same energy step within the same kinetic energy range; (4) setting an area analysis mode for acquiring AES spectrum as opposed to a point analysis mode that can cause serious damage to graphenes; (5) calibration of electron beam current by a Faraday cup before and after each measurement; (6) comparison of the intensities from graphenes with those from pure HOPG and/or pure substrate used for production of graphenes; and (7) maintaining the same measurement conditions. Despite these attentions and ultrahigh vacuum, AES measurement is quite simple for use and is easy to find interesting sample areas. It takes less than 5 min to obtain a high signal-to-noise spectroscopy and less than 60 min for a high signal-to-noise elemental map.

Acknowledgment. This work was partially supported by the budget for commission of MEXT, Japan, by the World Premier International Research Center Initiative (WPI Initiative) on Materials Nanoarchitectonics, MEXT, Japan, by the National Natural Science Foundation of China (Nos. 51011130028, 50990063, and 50973095). The authors thank Nanophoton Corp. for supporting Raman measurement.

Supporting Information Available: Calculation of IMFPs for graphite, comparison of AES spectra of monolayer graphene and HOPG in direct, first differential and second differential AES spectrum forms, reproducibility, AES spectra of graphene on Pt(111), SiC(0001), as well as transferred graphene onto SiO_2/Si from Ni. This material is available free of charge *via* the Internet at http://pubs.acs.org.

REFERENCES AND NOTES

1. Xia, F.; Mueller, T.; Lin, Y. M.; Valdes-Garcia, A.; Avouris, Ph. Ultrafast Graphene Photodetector. *Nat. Nanotechnol.* **2009**, *4*, 839–843.
2. Geim, A. K.; Novoselov, K. S. The Rise of Graphene. *Nat. Mater.* **2007**, *6*, 183–191.
3. Partoens, B.; Peeters, F. M. From Graphene to Graphite: Electronic Structure around the *K* Point. *Phys. Rev. B* **2006**, *74*, 075404.
4. Novoselov, K. S.; Geim, A. K.; Morozov, S. V.; Jiang, D.; Katsnelson, M. I.; Grigorieva, I. V.; Dubonos, S. V.; Firsov, A. A. Two-Dimensional Gas of Massless Dirac Fermions in Graphene. *Nature* **2005**, *438*, 197–200.
5. Zhang, Y.; Tan, Y. W.; Kim, P. Experimental Observation of the Quantum Hall Effect and Berry's Phase in Graphene. *Nature* **2005**, *438*, 201–204.
6. Berger, C.; Song, Z.; Li, X.; Wu, X.; Brown, N.; Naud, C.; Mayou, D.; Li, T.; Hass, J.; Marchenkov, A. N.; *et al.* Electronic Confinement and Coherence in Patterned Epitaxial Graphene. *Science* **2006**, *312*, 1191–1196.
7. McCann, E.; Fal'ko, V. I. Landau-Level Degeneracy and Quantum Hall Effect in a Graphite Bilayer. *Phys. Rev. Lett.* **2006**, *96*, 086805.
8. Semenoff, G. W. Condensed-Matter Simulation of a Three-Dimensional Anomaly. *Phys. Rev. Lett.* **1984**, *53*, 2449–2452.
9. McCann, E. Asymmetry Gap in the Electronic Band Structure of Bilayer Graphene. *Phys. Rev. B* **2006**, *74*, 161403.
10. Castro, E. V.; Novoselov, K. S.; Morozov, S. V.; Peres, N. M. R.; Lopes dos Santos, J. M. B.; Nilsson, J.; Guinea, F.; Geim, A. K.; Castro Neto, A. H. Biased Bilayer Graphene: Semiconductor with a Gap Tunable by the Electric Field Effect. *Phys. Rev. Lett.* **2007**, *99*, 216802.
11. Cracium, M. F.; Russo, S.; Yamamoto, M.; Oostinga, J. B.; Morpurgo, A. F.; Tarucha, S. Trilayer Graphene is a Semimetal with a Gate-Tunable Band Overlap. *Nat. Nanotechnol.* **2009**, *4*, 383–388.
12. Blake, P.; Hill, E. W.; Castro Neo, A. H.; Novoselov, K. S.; Jiang, D.; Yang, R.; Booth, T. J.; Geim, A. K. Making Graphene Visible. *Appl. Phys. Lett.* **2007**, *91*, 063124.
13. Friedemann, M.; Pierz, K.; Stosch, R.; Ahlers, F. J. Graphene on Gallium Arsenide: Engineering the Visibility. *Appl. Phys. Lett.* **2009**, *95*, 102103.
14. Gaskell, P. E.; Skulason, H. S.; Rodenchuk, C.; Szkopek, T. Counting Graphene Layers on Glass *via* Optical Reflection Microscopy. *Appl. Phys. Lett.* **2009**, *94*, 143101.
15. Ni, Z. H.; Wang, H. M.; Kasim, J.; Fan, H. M.; Yu, T.; Wu, Y. H.; Feng, Y. P.; Shen, Z. X. Graphene Thickness Determination Using Reflection and Contrast Spectroscopy. *Nano Lett.* **2007**, *7*, 2758–2763.
16. Casiraghi, C.; Hartschuh, A.; Lidorikis, E.; Qian, H.; Harutyunyan, H.; Gokus, T.; Novoselov, K. S.; Ferrari, A. C.

Rayleigh Imaging of Graphene and Graphene Layers. *Nano Lett.* **2007**, *7*, 2711–2717.
17. Ferrari, A. C.; Meyer, J. C.; Scardaci, V.; Casiraghi, C.; Lazzeri, M.; Mauri, F.; Piscanec, S.; Jiang, D.; Novoselov, K. S.; Roth, S.; *et al.* Raman Spectrum of Graphene and Graphene Layers. *Phys. Rev. Lett.* **2006**, *97*, 187401.
18. Gupta, A.; Chen, G.; Joshi, P.; Tadigadapa, S.; Eklund, P. C. Raman Scattering from High-Frequency Phonons in Supported *n*-Graphene Layer Films. *Nano Lett.* **2006**, *6*, 2667–2673.
19. Graf, D.; Molitor, F.; Ensslin, K.; Stampfer, C.; Jungen, A.; Hierold, C.; Wirtz, L. Spatially Resolved Raman Spectroscopy of Single- and Few-Layer Graphene. *Nano Lett.* **2007**, *7*, 238–242.
20. Calizo, I.; Bao, W.; Miao, F.; Lau, C. N.; Balandin, A. A. The Effect of Substrates on the Raman Spectrum of Graphene: Graphene-on-Sapphire and Graphene-on-Glass. *Appl. Phys. Lett.* **2007**, *91*, 201904.
21. Yoon, D.; Moon, H.; Son, W. Y.; Choi, J. S.; Park, B. H.; Cha, Y. H.; Kim, Y. D.; Cheong, H. Interference Effect on Raman Spectrum of Graphene on SiO_2/Si. *Phys. Rev. B* **2009**, *80*, 125422.
22. Calizo, I.; Bejenari, I.; Rahman, M.; Liu, G.; Balandin, A. A. Ultraviolet Raman Microscopy of Single and Multilayer Graphene. *J. Appl. Phys.* **2009**, *106*, 043509.
23. Ni, Z. H.; Chen, W.; Fan, X. F.; Kuo, J. L.; Yu, T.; Wee, A. T. S.; Shen, Z. X. Raman Spectroscopy of Epitaxial Graphene on a SiC Substrate. *Phy. Rev. B* **2008**, *77*, 115416.
24. Lee, D. S.; Riedl, C.; Krauss, B.; von Klitzing, K.; Starke, U.; Smet, J. H. Raman Spectra of Epitaxial Graphene on SiC and of Epitaxial Graphene Transferred to SiO_2. *Nano Lett.* **2008**, *8*, 4320–4325.
25. Calizo, I.; Ghosh, S.; Bao, W.; Miao, F.; Lau, C. N.; Balandin, A. A. Raman Nanometrology of Graphene: Temperature and Substrate Effects. *Solid State Commun.* **2009**, *149*, 1132–1135.
26. Ni, Z. H.; Yu, T.; Luo, Z. Q.; Wang, Y. Y.; Liu, L.; Wong, C. P.; Miao, J. M.; Huang, W.; Shen, Z. X. Probing Charged Impurities in Suspended Graphene Using Raman Spectroscopy. *ACS Nano* **2009**, *3*, 569–574.
27. Casiraghi, C.; Pisana, S.; Novoselov, K. S.; Geim, A. K.; Ferrari, A. C. Raman Fingerprint of Charged Impurities in Graphene. *Appl. Phys. Lett.* **2007**, *91*, 233108.
28. Casiraghi, C.; Hartschuh, A.; Qian, H.; Piscanec, S.; Georgi, C.; Fasoli, A.; Novoselov, K. S.; Basko, D. M.; Ferrari, A. C. Raman Spectroscopy of Graphene Edges. *Nano Lett.* **2009**, *9*, 1433–1441.
29. You, Y. M.; Ni, Z. H.; Yu, T.; Shen, Z. X. Edge Chirality Determination of Graphene by Raman Spectroscopy. *Appl. Phys. Lett.* **2008**, *93*, 163112.
30. Yu, T.; Ni, Z. H.; Du, C. L.; You, Y. M.; Wang, Y. Y.; Shen, Z. X. Raman Mapping Investigation of Graphene on Transparent Flexible Substrate: The Strain Effect. *J. Phys. Chem. C* **2008**, *112*, 12602–12605.
31. Huang, M. Y.; Yan, H. G.; Chen, C. Y.; Song, D. H.; Heinz, T. F.; Hone, J. Phonon Softening and Crystallographic Orientation of Strained Graphene Studied by Raman Spectroscopy. *Proc. Natl. Acad. Sci. U.S.A.* **2009**, *106*, 7304–7308.
32. Hao, Y.; Wang, Y.; Wang, L.; Ni, Z. H.; Wang, Z.; Wang, R.; Koo, C. K.; Shen, Z. X.; Thong, J. T. L. Probing Layer Number and Stacking Order of Few-Layer Graphene by Raman Spectroscopy. *Small* **2010**, *6*, 195–200.
33. Das, A.; Pisana, S.; Chakraborty, B.; Piscanec, S.; Saha, S. K.; Waghmare, U. V.; Novoselov, K. S.; Krishnamurthy, H. R.; Geim, A. K.; Ferrari, A. C.; *et al.* Monitoring Dopants by Raman Scattering in an Electrochemically Top-Gated Graphene Transistor. *Nat. Nanotechnol.* **2008**, *3*, 210–215.
34. Yan, J.; Zhang, Y. B.; Kim, P.; Pinczuk, A. Electric Field Effect Tuning of Electron−Phonon Coupling in Graphene. *Phys. Rev. Lett.* **2007**, *98*, 166802.
35. Levendorf, M. P.; Ruiz-Vargas, C. S.; Garg, S.; Park, J. Transfer-Free Batch Fabrication of Single Layer Graphene Transistors. *Nano Lett.* **2009**, *9*, 4479–4483.
36. Sutter, P. W.; Flege, J. I.; Sutter, E. S. Epitaxial Graphene on Ruthenium. *Nat. Mater.* **2008**, *7*, 406–411.
37. Reina, A.; Thiele, S.; Jia, X.; Bhaviripudi, S.; Dresselhaus, M. S.; Scharfer, J. A.; Kong, J. Growth of Large-Area Single- and Bi-Layer Graphene by Controlled Carbon Precipitation on Polycrystalline Ni Surfaces. *Nano Res.* **2009**, *2*, 509–516.
38. Preobrajenski, A. B.; Ng, M. L.; Vinogradov, A. S.; Martensson, N. Controlling Graphene Corrugation on Lattice-Mismatched Substrates. *Phys. Rev. B* **2008**, *78*, 073401.
39. Yu, Q. K.; Lian, J.; Siriponglert, S.; Li, H.; Chen, Y. P.; Pei, S. S. Graphene Segregated on Ni Surfaces and Transferred to Insulators. *Appl. Phys. Lett.* **2008**, *93*, 113103.
40. Reina, A.; Jia, X. T.; Ho, J.; Nezich, D.; Son, H. B.; Bulovic, V.; Dresselhaus, M. S.; Kong, J. Large Area, Few-Layer Graphene Films on Arbitrary Substrates by Chemical Vapor Deposition. *Nano Lett.* **2009**, *9*, 30–35.
41. Kim, K. S.; Zhao, Y.; Jang, H.; Lee, S. Y.; Kim, J. M.; Kim, K. S.; Ahn, J. H.; Kim, P.; Choi, J. Y.; Hong, B. H. Large-Scale Pattern Growth of Graphene Films for Stretchable Transparent Electrodes. *Nature* **2009**, *457*, 706–710.
42. Li, X.; Cai, W.; An, J.; Kim, S.; Nah, J.; Yang, D. X.; Piner, R.; Velamakanni, A.; Jung, I.; Tutuc, E.; *et al.* Large-Area Synthesis of High-Quality and Uniform Graphene Films on Copper Foils. *Science* **2009**, *324*, 1312–1314.
43. Li, X.; Cai, W.; Colombo, L.; Ruoff, R. S. Evolution of Graphene Growth on Ni and Cu by Carbon Isotope Labeling. *Nano Lett.* **2009**, *9*, 4268–4272.
44. Briggs, D., Seah, M. P., Eds. *Practical Surface Analysis. Auger and X-ray Photoelectron Spectroscopy*, 2nd version; John Wiley & Sons: New York, 1984; Vol. 1.
45. Shelton, J. C.; Patil, H. R.; Blakely, J. M. Equilibrium Segregation of Carbon to a Nickel(111) Surface−Surface Phase-Transition. *Surf. Sci.* **1974**, *43*, 493–520.
46. Fujita, D.; Schleberger, M.; Tougaard, S. Extraction of Depth Distributions of Electron-Excited Auger Electrons in Fe, Ni and Si Using Inelastic Peak Shape Analysis. *Surf. Sci.* **1996**, *357*, 180–185.
47. Fujita, D.; Homma, T. Surface Precipitation of Graphite Layers on Carbon-Doped Nickel and Their Stabilization Effect against Chemisorption Oxidation. *Surf. Interface Anal.* **1992**, *19*, 430–434.
48. Berger, C.; Song, Z.; Li, T.; Li, X. B.; Ogbazghi, A. Y.; Feng, R.; Dai, Z.; Marchenkov, A. N.; Conrad, E. H.; First, P. N.; de Heer, W. A. Ultrathin Epitaxial Graphite: 2D Electron Gas Properties and a Route toward Graphene-Based Nanoelectronics. *J. Phys. Chem. B* **2004**, *108*, 19912–19916.
49. Belobrov, P. I.; Bursill, L. A.; Maslakov, K. I.; Dementjev, A. P. Electron Spectroscopy of Nanodiamond Surface States. *Appl. Surf. Sci.* **2003**, *215*, 169–177.
50. Charlier, J. C.; Gonze, X.; Michenaud, J. P. 1st-Principles Study of the Electronic-Properties of Graphite. *Phys. Rev. B* **1991**, *43*, 4579–4589.
51. Chung, D. D. L. Review Graphite. *J. Mater. Sci.* **2002**, *37*, 1475–1489.
52. Krauss, B.; Lohmann, T.; Chae, D. H.; Haluska, M.; von Klitzing, K.; Smet, J. H. Laser-Induced Disassembly of a Graphene Single Crystal into a Nanocrystalline Network. *Phys. Rev. B* **2008**, *79*, 165428.
53. Gergely, G. Elastic Backscattering of Electrons: Determination of Physical Parameters of Electron Transport Processes by Elastic Peak Electron Spectroscopy. *Prog. Surf. Sci.* **2002**, *71*, 31–88.
54. Tanuma, S.; Powell, C. J.; Penn, D. R. Calculations of Electron Inelastic Mean Free Paths. 2. Data for 27 Elements over the 50−2000 eV Range. *Surf. Interface Anal.* **1991**, *17*, 911–926.
55. Nemes-Incze, P.; Osvath, Z.; Kamaras, K.; Biro, L. P. Anomalies in Thickness Measurements of Graphene and Few Layer Graphite Crystals by Tapping Mode Atomic Force Microscopy. *Carbon* **2008**, *46*, 1435–1442.
56. Rosei, R.; De Crescensti, M.; Sette, F.; Quaresima, C.; Savoia, A.; Perfetti, P. Structure of Graphitic Carbon on Ni(111): A Surface Extended-Energy-Loss Fine-Structure Study. *Phys. Rev. B* **1983**, *28*, 1161–1164.

57. Nagashima, A.; Tejima, N.; Oshima, C. Electronic States of the Pristine and Alkali-Metal-Intercalated Monolayer Graphite/Ni(111) Systems. *Phys. Rev. B* **1994**, *50*, 17487–11495.
58. de Heer, W. A.; Berger, C.; Wu, X.; First, P. N.; Conrad, E. H.; Li, X.; Li, T.; Sprinkle, M.; Hass, J.; Sadowsski, M. L.; *et al.* Epitaxial Graphene. *Solid State Commun.* **2007**, *143*, 92–100.
59. Gao, J. H.; Fujita, D.; Xu, M. S.; Onishi, K.; Miyamoto, S. Unique Synthesis of Few-Layer Graphene Films on Carbon-Doped $Pt_{83}Rh_{17}$ Surfaces. *ACS Nano* **2010**, *4*, 1026–1032.
60. Xu, M. S.; Pathak, Y.; Fujita, D.; Ringo, C.; Miyazawa, K. Covered Conduction of Individual C_{60} Nanowhiskers. *Nanotechnology* **2008**, *19*, 075712.
61. Geim, A. K. Graphene: Status and Prospects. *Science* **2009**, *324*, 1530–1534.